



Identification of potent pan-ephrin receptor kinase inhibitors using DNA-encoded chemistry technology

Chandrashekhar Madasu^{a,b,1}, Zian Liao^{a,b,c,1} , Sydney E. Parks^{a,b}, Kiran L. Sharma^{a,b} , Kurt M. Bohren^{a,b} , Qiuji Ye^{a,b} , Feng Li^{a,b,d} , Murugesan Palaniappan^{a,b} , Zhi Tan^{a,b,d}, Fei Yuan^{a,b}, Chad J. Creighton^{e,f,g}, Suni Tang^{a,b}, Ramya P. Masand^{a,h}, Xiaoming Guan^h, Damian W. Young^{a,b,d}, Diana Monsivais^{a,b,2}, and Martin M. Matzuk^{a,b,c,d,2}

Contributed by Martin M. Matzuk; received December 28, 2023; accepted March 22, 2024; reviewed by Thomas D. Chung and Yikai Wang

EPH receptors (EPHs), the largest family of tyrosine kinases, phosphorylate downstream substrates upon binding of ephrin cell surface–associated ligands. In a large cohort of endometriotic lesions from individuals with endometriosis, we found that *EPHA2* and *EPHA4* expressions are increased in endometriotic lesions relative to normal eutopic endometrium. Because signaling through EPHs is associated with increased cell migration and invasion, we hypothesized that chemical inhibition of EPHA2/4 could have therapeutic value. We screened DNA-encoded chemical libraries (DECL) to rapidly identify EPHA2/4 kinase inhibitors. Hit compound, CDD-2693, exhibited picomolar/nanomolar kinase activity against EPHA2 (K_i : 4.0 nM) and EPHA4 (K_i : 0.81 nM). Kinome profiling revealed that CDD-2693 bound to most EPH family and SRC family kinases. Using NanoBRET target engagement assays, CDD-2693 had nanomolar activity versus EPHA2 (IC_{50} : 461 nM) and EPHA4 (IC_{50} : 40 nM) but was a micromolar inhibitor of SRC, YES, and FGR. Chemical optimization produced CDD-3167, having picomolar biochemical activity toward EPHA2 (K_i : 0.13 nM) and EPHA4 (K_i : 0.38 nM) with excellent cell-based potency EPHA2 (IC_{50} : 8.0 nM) and EPHA4 (IC_{50} : 2.3 nM). Moreover, CDD-3167 maintained superior off-target cellular selectivity. In 12Z endometriotic epithelial cells, CDD-2693 and CDD-3167 significantly decreased EFNA5 (ligand) induced phosphorylation of EPHA2/4, decreased 12Z cell viability, and decreased IL-1 β -mediated expression of prostaglandin synthase 2 (*PTGS2*). CDD-2693 and CDD-3167 decreased expansion of primary endometrial epithelial organoids from patients with endometriosis and decreased Ewing's sarcoma viability. Thus, using DECL, we identified potent pan-EPH inhibitors that show specificity and activity in cellular models of endometriosis and cancer.

DNA-encoded chemistry | ephrin receptor kinase inhibitors | endometriosis

Ephrin ligands (EFN) and ephrin binding cell-surface receptors (EPH) play crucial roles in various biological processes, from early development to maintenance of tissue homeostasis (1–4). EFN ligands are grouped into EFNA and EFNBs based on structural similarities and anchoring to the cell membrane. EPH receptors are further subcategorized into EPHA or EPHB subcategories based on sequence homology and preferential binding to corresponding EFNA or EFNB ligands. EFN-EPH signaling pathways are critical in cell-to-cell communication and guidance, particularly in the context of neuronal migration and synapse formation during physiological and disease conditions (5, 6).

Endometriosis, a condition which burdens more than 190 million women globally, is defined as the abnormal appearance of endometrial tissues outside of the uterine cavity (7). It is characterized by prolonged inflammation, contributing to significant morbidity in women. Endometriosis not only causes dysmenorrhea and chronic pelvic pain, it also leads to infertility and increased risk for ovarian cancer (8). Currently, treatment options for endometriosis are limited to surgical removal of the endometrial lesions, nonsteroidal anti-inflammatory drugs (NSAIDs), and oral contraceptives for pain management (9). However, these treatment options are associated with significant challenges, including limited efficacy, fertility concerns, and recurrent symptoms. The gap in the high prevalence and limited therapeutic options of endometriosis provide a compelling rationale for identifying innovative and effective drug targets. Previous studies indicate that endometrial cells express EFN ligands and EPH receptors and have critical roles in endometrial repair (10), embryo implantation (11–14), and endometrial cancer (15–17). EFN signaling is also critical in the control of ovarian function, where the expression of prostaglandin synthase 2 (*PTGS2*) and other genes critical for folliculogenesis (18). In endometriosis, blocking of EPHA2 using antibody-based or CRISPR knockout strategies was found to decrease the cytotoxicity of gamma delta T cells derived from patients with endometriosis, suggesting that EPHA2 inhibition is a possible therapeutic intervention for endometriosis (19). Hence,

Significance

EPH receptors (EPHs) are highly sought-after drug targets owing to their essential roles in maintaining appropriate cellular functions in both physiological and disease conditions. However, limited potency and specificity pose significant obstacles to the development of small-molecule inhibitors for EPHs. Here, using high-throughput DNA-encoded chemical library screenings, we developed potent and selective inhibitors of the EPH receptor kinase family. Our results also emphasize the therapeutic potential of our EPH inhibitors in cancer and endometriosis, a global health concern that causes chronic pain and often leads to infertility in women. This study showcases the robust pipeline of using DNA-encoded chemistry technology to identify nonhormonal therapeutic agents tailored for the treatment of gynecologic diseases, including, but not limited to, endometriosis.

Reviewers: T.D.C., Sanford Burnham Prebys Medical Discovery Institute; and Y.W., Keen Therapeutics.

The authors declare no competing interest.

Copyright © 2024 the Author(s). Published by PNAS. This article is distributed under [Creative Commons Attribution-NonCommercial-NoDerivatives License 4.0 \(CC BY-NC-ND\)](#).

¹C.M. and Z.L. contributed equally to this work.

²To whom correspondence may be addressed. Email: diana.monsivais@bcm.edu or mmatzuk@bcm.edu.

This article contains supporting information online at <https://www.pnas.org/lookup/suppl/doi:10.1073/pnas.2322934121/-DCSupplemental>.

Published May 3, 2024.

EFN-EPH signaling is crucial for many aspects of reproductive function and is altered in various gynecological diseases, making EFN-EPH signaling pathways important therapeutically (20).

EFN-EPH signaling is also implicated in cancer pathogenesis and progression through their modulation of cell migration and invasion, as well as their role in promoting angiogenesis (21). Among the cancer types found to be critically modulated by the expression of EPH family members is Ewing sarcoma, a rare pediatric bone sarcoma with poor patient outcomes (22). EPHA2 expression is up-regulated in Ewing sarcoma tissues, and increased expression of EPHA2 is crucial for promoting angiogenesis in this cancer (23, 24).

Efforts have previously been made in generating EFN/EPH targeting molecules. Multiple strategies have been utilized, including blocking EPH receptor interactions using protein-based antagonists (25–27), down-regulating EPH expression levels (28–30), and inhibiting the kinase domain through the addition of ATP-binding competitors (31–33). However, varying potency and limited specificity toward EPHs were observed in these targeting molecules, which led us to focus on synthesizing effective small-molecule kinase inhibitors for the EPH family of proteins.

The development of novel drugs typically relies on identifying high-affinity small molecules that can bind selectively to proteins of interest and modulate the biological target. For hit identification, high-throughput screening has been a leading platform for providing molecular starting points; however, it can be costly and time-consuming. In recent years, DNA-encoded chemistry technology (DEC-Tec) has emerged as a powerful and promising alternative screening platform for discovering new small-molecule hits for a wide range of therapeutic kinase targets with exceptional speed and cost-effectiveness (34–37). The production of DNA-encoded chemical libraries (DECLs) is based on a split-and-pool strategy with sequential cycles of combinatorial chemistry and DNA ligation yielding an average library size of ~100 million compounds. The large number of compounds arises from incorporating a large number of building blocks (BBs).

The hit molecules in DECLs comprise a large-scale collection of diverse BBs assembled in a combinatorial fashion. Every molecule is covalently bonded to the unique conjugated DNA sequence, acting as an identification barcode (38). The DECL screening typically involves the affinity selection of libraries, which can yield specific binders to diverse target proteins. Each library is characterized by a distinct core scaffold containing a unique 3-codon amplifiable DNA barcode, making it easier to identify structural information and enabling next-generation DNA sequencing, data analysis, and hit confirmation. Following the interpretation of the screening results, the strong binders or hit candidates are synthesized in an off-DNA approach for biochemical testing (39). To date, several potent hit molecules have been reported from our group for specific targets, including bromodomain testis (BRDT) (40, 41), bone morphogenic protein receptor type 2 (BMPR2) (42), and SARS-CoV-2 main protease (Mpro) (43). Based on the merits of DEC-Tec, we applied it for identifying inhibitors of EPHA2 and EPHA4 which we established as relevant targets in endometriosis.

In the present study, we report the identification of potent EPH kinase inhibitors using DEC-Tec screening of a multibillion compound collection with an EPHA4 kinase domain. After analysis of the enrichment selection profile, we identified related hits from two distinct libraries and confirmed the activities of the hits when synthesized off-DNA and tested in biochemical and cellular assays. Hit compounds and their representative analogs demonstrated excellent inhibition and showed exceptional cellular pan-EPH kinase selectivity. Herein, we present our initial use of these pan-EPH kinase inhibitors for exploring EPH functions *in vitro* in models of endometriosis and cancer.

Results

EPHA2 and EPHA4 Are Increased in Endometriotic Lesions from Patients with Endometriosis. Given the prevalence of kinase inhibitors as FDA-approved drugs, we wondered whether certain kinases might be therapeutic targets in endometriosis. Accordingly, we performed an analysis of overexpressed kinases in endometriotic lesions from peritoneal endometriosis lesion (PeL, N = 71), deep infiltrating endometriosis (DiE, N = 167), and endometriomas (OMA, N = 25) relative to normal eutopic endometrial tissues (CE, N = 43) and the patient endometrium (PE, N = 104) from a previously published dataset (GSE141549) (44). We identified *EPHA2* and *EPHA4* as potential nonhormonal therapeutic targets for endometriosis based on their significantly elevated expression levels in the PeL and DiE relative to CE (Fig. 1A and B and *SI Appendix*, Fig. S1A). In endometrioma tissues (OMA),

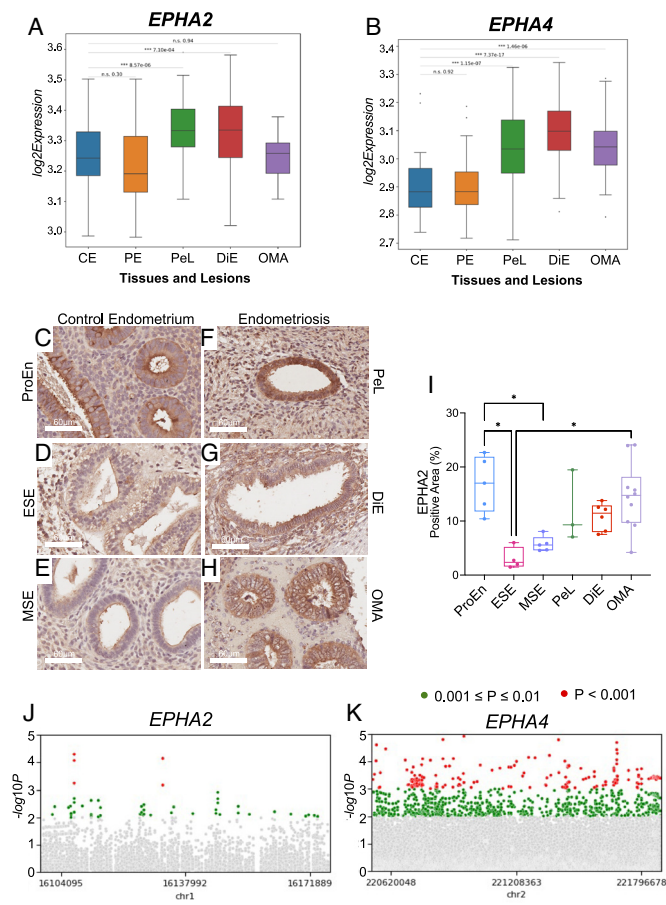


Fig. 1. Identification of EPHA2 and EPHA4 as drug targets in endometriosis. (A and B) Expression levels of *EPHA2* (A) and *EPHA4* (B) were determined from GSE141549 and represent samples from CE (N = 43); PE (N = 104); PeL (N = 71); DiE (N = 167); and OMA (N = 25). Box and whisker plots represent $\log_2\text{Expression}$ and are plotted as mean, with min-max expression. Lesion expression was evaluated using multiple testing ($FDR < 0.05$) in CE versus PeL, OMA, and DiE. (C–H) EPHA2 immunohistochemistry (IHC) in CE obtained from proliferative phase (C, ProEN, N=5), early secretory endometrium (D, ESE, N = 4) and midsecretory endometrium (E, MSE, N = 5). EPHA2 was also assessed in PeL (N = 3), DiE (N = 6), and OMA (N = 10). White boxes represent the areas presented with a higher magnification. (I) Quantification of the EPHA2 signal in the various lesions was determined using ImageJ and presented as the percent area analyzed with positive signal. Data are presented as box and whisker plots with min-max expression and analyzed using a Kruskal-Wallis test with a Dunnett's multiple comparison posttest. (J and K) Analysis of 36,697 endometriosis cases and 116,071 controls from the FinnGen database identified 5 *EPHA2* (J) and 210 *EPHA4* (K) variants associated with endometriosis ($P < 0.001$, in red). NOTE: 54 *EPHA2* and 1049 *EPHA4* variants are found with $0.001 \leq P \leq 0.01$, in green. Variants within the *EPHA2/EPHA4* gene boundaries are darker, and those up/downstream of the *EPHA2/EPHA4* gene boundaries are displayed in lighter colors.

EPHA4 was 1.74-fold higher ($FDR < 0.001$) relative to control endometrium (CE); in peritoneal lesions (PeL), *EPHA2* was 1.57-fold ($FDR < 0.001$) and *EPHA4* was 1.72-fold ($P < 0.001$) higher than CE; while in deep infiltrating endometriotic lesions (DiE), *EPHA2* was 1.34-fold ($FDR < 0.01$), and *EPHA4* was 1.75-fold ($FDR < 0.001$) higher than in CE. Using this approach, we identified *EPHA2* and *EPHA4* as kinase receptors up-regulated in a large set of endometriotic lesions relative to CE.

Endometrial EPHA2 and EPHA4 Expression Changes during the Menstrual Cycle, and the Proteins Localize to the Endometrial and Endometriotic Stroma and Epithelium. To determine whether the levels of *EPHA2* and *EPHA4* changed throughout the menstrual cycle, we analyzed a gene expression dataset (GSE51981) of endometrial biopsies staged according to the menstrual cycle phase (45). Levels of *EPHA2* are significantly decreased in the early secretory ($N = 6$) and midsecretory ($N = 8$) endometrium relative to the proliferative endometrial biopsies ($N = 20$) (SI Appendix, Fig. S1B). On the other hand, *EPHA4* levels are increased in the early secretory and midsecretory endometrium relative to the proliferative phase endometrium (SI Appendix, Fig. S1C). Thus, the levels of *EPHA2* and *EPHA4* dynamically change in the eutopic normal endometrium.

EPHA2 Is Expressed in the Normal Eutopic Endometrium and in Endometriotic Lesions. To validate the expression levels and localization of EPHA2 in the normal endometrium and endometriotic lesions, we performed EPHA2 IHC in the normal

eutopic endometrium (CE, $N = 15$), peritoneal endometriotic lesions (PeL, $N = 3$), deep infiltrating endometriosis (DiE, $N = 6$), and in OMA ($N = 10$) (Fig. 1 C–H). IHC in the normal eutopic endometrium was performed using biopsies obtained during various phases of the menstrual cycle, using proliferative endometrium (ProEn, $N = 5$), early secretory endometrium (ESE, $N = 4$), and midsecretory endometrium (MSE, $N = 5$). We found that relative to the proliferative phase endometrium, EPHA2 levels decreased in the ESE (Fig. 1I). Likewise, relative to the ESE normal endometrium, levels of EPHA2 were significantly elevated in the endometrioma tissues (Fig. 1J). Compartment-specific analyses identified that EPHA2 was more frequently detected in the epithelial layers of the lesion; however, some lesions also displayed high EPHA2 expression in the stroma. Thus, our results here validate the microarray analyses, showing that EPHA2 is detected in the epithelium and stromal cell compartments of the endometriotic lesions and the normal eutopic endometrium. We also demonstrate that EPHA2 levels fluctuate in the normal eutopic endometrium.

Genetic Variants of EPHA2 and EPHA4 Are Enriched in Patients with Endometriosis. We also identified many *EPHA2* and *EPHA4* variants that were associated with endometriosis (Fig. 1 J and K). The analysis was performed in a cohort of 36,697 endometriosis cases and 116,071 controls annotated in the FinnGen database (46). We found that approximately five variants associated with *EPHA2* and 210 variants associated with *EPHA4* with a cutoff of $P < 0.001$ (displayed in red), while 54 variants associated with *EPHA2* and 1,049 variants associated with *EPHA4* with a cutoff

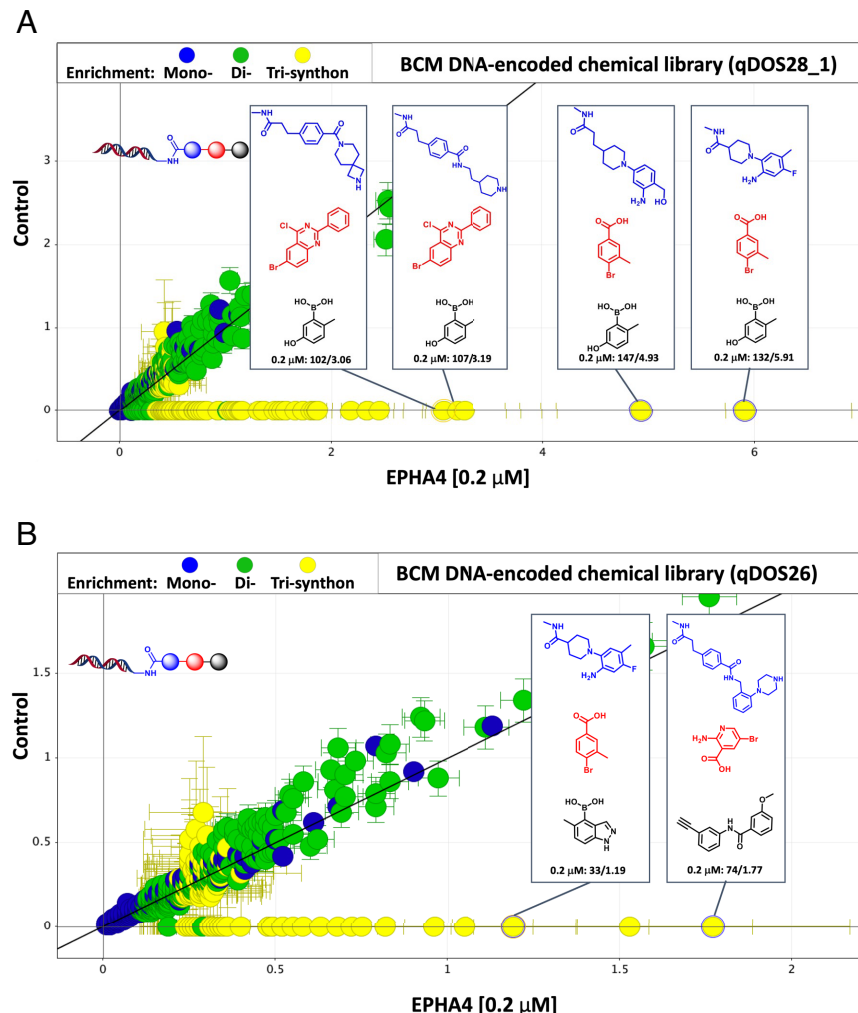
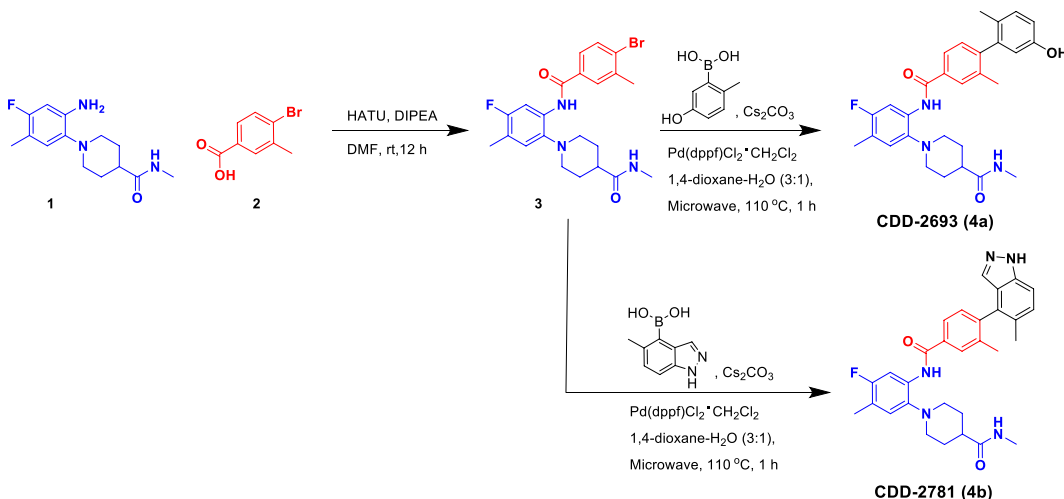


Fig. 2. DECL selection data (A) qDOS28_1 and (B) qDOS26. The enrichment of each library series was shown as count/z-score in the box and graphed as z-score in the EPHA4 0.2 μ M selection on the x axis versus z-score for the selection against non-target control on the y axis. For each library, the structures BB1 (in blue), BB2 (in red), and BB3 (in black) are shown from the Top to Bottom. The desired chemical structures of strongly enriched hit compounds CDD-2693 and CDD-2781 are shown on the Right.



Scheme 1. Off-DNA synthesis of DEC-Tec selection hits (CDD-2693 and CDD-2781).

of $0.001 \leq P \leq 0.01$. Thus, our analysis reveals that *EPHA2* and *EPHA4* display increased gene expression and increased genetic variants that are associated with endometriosis.

DEC-Tec Affinity Selection with EPHA2 and EPHA4 Proteins.

To identify potent and selective small molecules that inhibit the kinase activity of EPHA2 and EPHA4, 54 unique DECLs cumulatively containing 4.42 billion compounds were screened in our DEC-Tec platform with an *N*-terminal-His-tagged EPHA2

kinase domain (amino acids 596 to 900) or EPHA4 kinase domain (amino acids 601 to 892) that were produced in insect cells. During affinity selections, library pools were incubated with His-tagged EPHA2 or EPHA4 at a concentration of 0.2 μM. A no-target control (NTC) experiment without target protein was also performed in parallel as a negative control to rule out nonspecific bead binders. After three to four rounds of selection, NTC, EPHA2, and EPHA4 samples were PCR amplified and subjected to Illumina next-generation sequencing. Our informatics pipeline was used to decode the chemical structures bound to EPHA2 and EPHA4 from DNA sequences captured by the sequencer and to calculate the enrichment of these compounds through statistical analysis. Enrichment of the EPHA4 bound compounds is shown in Fig. 2 with their normalized z-score and number of counts. We developed an in-house normalized z-score to quantify the enrichment of n-synthons to address the bias of count data caused by factors such as sample size and library diversity (38). A higher z-score indicates a more significant enrichment in the selection.

Analysis of the compounds from two libraries, qDOS28_1 and qDOS26, indicated that structurally similar molecules were enriched (Fig. 2). In addition to normalized z-scores, the analysis of enriched compounds that are structurally similar gives further credence that the compounds are real binders, while also informing on structural features involved in target recognition. Hit compounds CDD-2693 (MW: 489) and CDD-2781 (MW: 513), identified from qDOS28_1 and qDOS26, respectively, were synthesized off-DNA and shown to be potent inhibitors of EPHA2 and EPHA4 in vitro as presented in the next sections.

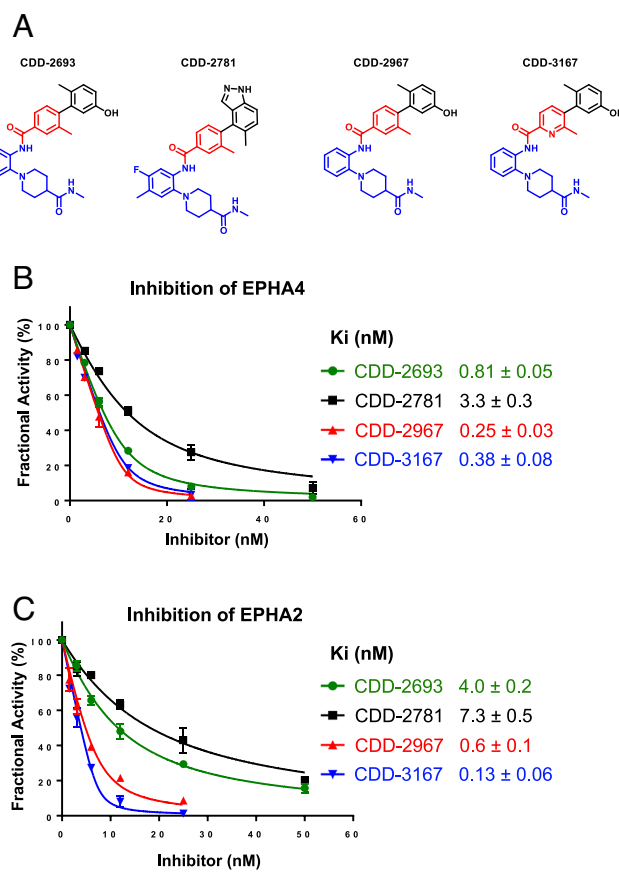


Fig. 3. Inhibition of selected compounds against EPHA4 and EPHA2. (A) Chemical structures of potent compounds. (B) Dose-response curves of represented compounds against EPHA4. (C) Dose-response curves of represented compounds against EPHA2.

Validation and Synthesis of DEC-Tec Selection Hits (CDD-2693 and CDD-2781). After DEC-Tec selection, we analyzed the BB combinations according to the most enriched sequences. This analysis revealed two compounds, CDD-2693 and CDD-2781 (encoded from libraries qDOS28_1 and qDOS26, respectively), having identical structures for BB1 and BB2 but differing in BB3. The structural similarity of the two compounds arising from two distinct libraries provided confidence for validating them by off-DNA synthesis.

The chemical synthesis of DEC-Tec hit compounds is shown in Scheme 1. In brief, the synthesis of CDD-2693 initiated by amide coupling of readily available (1-(2-amino-4-fluoro-5-methylphenyl)-N-methylpiperidine-4-carboxamide (**1**) and 4-bromo-3-methylbenzoic acid (**2**) to provide key precursor (**3**). Subsequently, a Suzuki-Miyaura coupling was performed between arylbromomide intermediate **3** and 5-hydroxy-2-methylphenyl boronic acid to yield the desired target compound CDD-2693

Table 1. Kinase selectivity data for compounds CDD-2693 and CDD-3167

Kinases	CDD-2693 K_i (nM)	CDD-3167 K_i (nM)	Kinases	CDD-2693 K_i (nM)	CDD-3167 K_i (nM)
EPHA1	2.1	4.0	EPHB3	128	4.9
EPHA2	4.0	0.1	EPHB4	4.8	0.3
EPHA3	45	2.1	FGR	1.8	1.1
EPHA4	0.8	0.4	FRK	9.4	5.2
EPHA5	1.0	0.7	LCK	10.6	1.0
EPHA6	186	1.6	LYNA	11.8	0.8
EPHA7	NA	29	SRC	11.9	0.7
EPHA8	4.7	0.2	TXK	17.8	4.0
EPHB1	2.0	0.5	YES1	2.0	0.2
EPHB2	1.3	0.2	BLK	8.8	0.4

NA, not active at 1 μ M in the Z'-LYTE and Adapta inhibition data

(4a, 51%). Similarly, intermediate 3 was reacted with (5-methyl-1H-indazol-4-yl)boronic acid to furnish the hit compound CDD-2781 (4b) in 36% yield. Further confirmation of the binding of hit candidate CDD-2693 in the EPHA2 and EPHA4 kinase domain, we used a thermal shift assay (TSA) to measure the extent of protein stabilization induced by small-molecule binding (*SI Appendix*, Fig. S2). To examine the inhibitory activity of the resulting hit candidates, we screened for EPHA4 and EPHA2 kinase domains using an in vitro biochemical assay (Fig. 3). The CDD-2693 displayed picomolar/nanomolar potency [EPHA4 (K_i : 0.8 nM), EPHA2 (K_i : 4.0 nM)], and another hit candidate CDD-2781 [EPHA4 (K_i : 3.3 nM), EPHA2 (K_i : 7.3 nM)] displayed nanomolar potency. These biochemical data highlight that DEC-Tec can provide exceptionally potent compounds directly from the selection and without the need for extensive medicinal chemistry efforts.

Kinase Selectivity Profile of CDD-2693. To interrogate the kinome-wide selectivity of CDD-2693, we performed a KINOMEscan assay at Eurofins at 1 μ M concentration toward a panel of 468 kinases (31, 47). The KINOMEscan (Fig. 4) revealed CDD-2693 to be selective across the human kinome, inhibiting only closely related EPH and SRC tyrosine kinase (TK) family members (*SI Appendix*, Table S1). To further confirm this selectivity, we conducted a LanthaScreen kinase binding assay on selective EPH and SRC kinase targets using Thermo Fischer Scientific's SelectScreenServices (Table 1). CDD-2693 demonstrated nanomolar potency against EPHA2 (K_i : 4.0 nM), EPHA4 (K_i : 0.8 nM), EPHA8 (K_i : 4.7 nM), and EPHB4 (K_i : 4.8 nM). Additionally, CDD-2693 also displayed nanomolar potency toward a branch of nonreceptor SRC tyrosine protein kinases, including FGR (K_i : 1.8 nM), YES1 (K_i : 2.0 nM), BLK (K_i : 8.8 nM), FRK (K_i : 9.4 nM), LCK (K_i : 10.6 nM), LYNA (K_i : 11.8 nM), and SRC (K_i : 11.9 nM). This underscores that in addition to generating potent compounds, DEL selections can also identify compounds with admirable selectivity.

Exploration of Structure-Activity Relationship (SAR). Having achieved excellent inhibition of EPHA2 and EPHA4 directly from the DEL selection, we next synthesized derivative compounds and performed computational modeling to explore SAR and understand the structural features required for activity. Additionally, we sought to produce compounds with further potency, greater off-target selectivity, and better drug-like properties such as solubility and metabolic stability. Given the modularity of DELs, off-DNA SAR could be efficiently determined through the incorporation of BBs

having specific structural features without changing the synthetic pathway outlined in Scheme 1. We mainly focused on varying the substituents on the two aromatic rings (A-ring and B-ring) contained in the parent compounds CDD-2693 and CDD-2781 (Table 2). To generate analogs with greater solubility for better cell penetration, we explored truncations at the A-ring R_3 site close to the former DNA attachment point. Removal of the entire methylpiperidine-4-carboxamide (R_3) group (CDD-2868) resulted in a complete loss of activity to both EPHA2 and EPHA4 as did truncation down to the dimethylamine (CDD-2903). Furthermore, eliminating just the N-methycarboxamide portion from the piperidine ring (CDD-2869 and CDD-2904) also ablated activity. These results suggested that the N-methycarboxamide forms critical interactions to EPHA4 and EPHA2. Our modeling results show that the nitrogen in the N-methycarboxamide moiety forms hydrogen bonds with Arg750 and Ser706 in EPHA4. Intriguingly, this serine is absent in EPHA2, being replaced by Ala599. This may partially explain why this series of compounds showed better binding affinity to EPHA4 in comparison to EPHA2 (Fig. 5). We next prepared analogs with varying substituents at the R_1 and R_2 positions of the A-ring. Eliminating the R_2 fluoro group (CDD-2905) yielded similar potency but a turnover in selectivity given that better potency to EPHA2 (K_i : 1.0 nM) over EPHA4 (K_i : 5 nM) was observed. Substitution with the smaller N-methycarboxamide at R_3 of the defluorinated compounds (CDD-2969 and CDD-2970) diminished the EPH activities once again corroborating the importance of the entire N-methylpiperidine-4-carboxamide unit. CDD-2967 which lacks both the fluoro and methyl groups at R_1 and R_2 relative to the parent (CDD-2693), gave K_i values of 0.6 nM and 0.25 nM to EPHA2 and EPHA4,

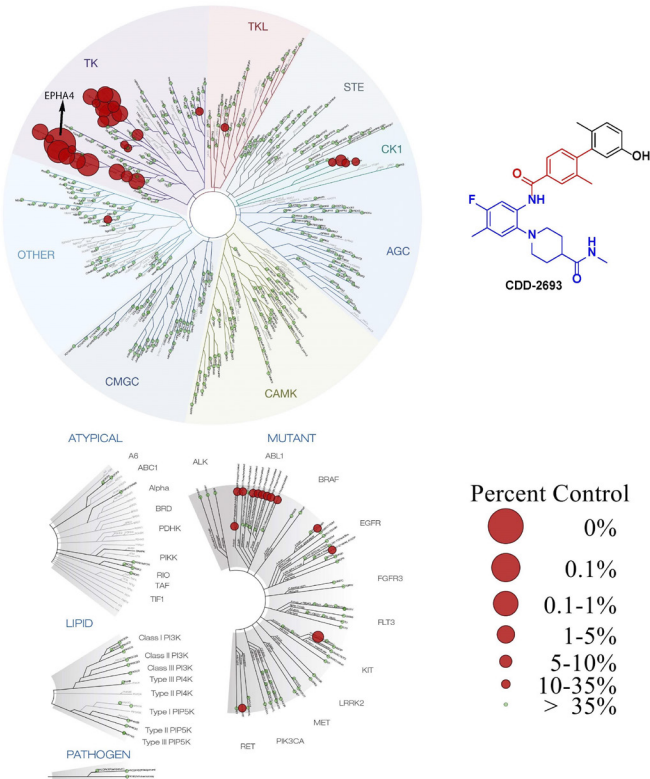


Fig. 4. Selectivity profile of compound CDD-2693 was assayed at 1 μ M against 468 kinases using the DiscoveRx KINOMEscan screen. Compound selectivity is represented in a TREEspot kinase dendrogram view of the human kinome phylogenetic tree. Inhibition was measured in the percentage of control; the lower the percent control and the larger the red circles indicate stronger inhibition against the corresponding kinases; all other kinases tested were inactive, as indicated by the green circles.

Table 2. Structures and activities of hits (CDD-2693 and CDD-2781) and SAR analogs

Compound	R ₁	R ₂	R ₃	X	R ₄	R ₅	EPHA4 (K _i , nM)	EPHA2 (K _i , nM)
CDD-2693 (4a)	F	CH ₃		CH	CH ₃		0.81 ± 0.05	4.0 ± 0.2
CDD-2781 (4b)	F	CH ₃		CH	CH ₃		3.3 ± 0.3	7.3 ± 0.5
CDD-2868 (4c)	F	CH ₃	H	CH	CH ₃		NA	NA
CDD-2869 (4d)	F	CH ₃		CH	CH ₃		NA	NA
CDD-2903 (4e)	F	CH ₃		CH	CH ₃		NA	NA
CDD-2904 (4f)	F	CH ₃		CH	CH ₃		NA	NA
CDD-2905 (4g)	H	CH ₃		CH	CH ₃		5.0 ± 1.2	1 ± 0.4
CDD-2967 (4h)	H	H		CH	CH ₃		0.25 ± 0.05	0.6 ± 0.1
CDD-2968 (4i)	H	H		CH	CH ₃		9.7 ± 1.6	0.7 ± 0.3
CDD-2969 (4j)	H	CH ₃		CH	CH ₃		6.7 ± 1.8	22.5 ± 4.1
CDD-2970 (4k)	H	CH ₃		CH	CH ₃		5.5 ± 0.8	14.1 ± 2.6
CDD-3074 (4l)	H	H		CH	CH ₃		17.7 ± 1.6	53 ± 18
CDD-3075 (4m)	H	H		CH	CH ₃		NA	NA
CDD-3076 (4n)	H	H		CH	CH ₃		NA	NA

Table 2. (Continued)

Compound	R ₁	R ₂	R ₃	X	R ₄	R ₅	EPHA4 (K _i , nM)	EPHA2 (K _i , nM)
CDD-3163 (4o)	H	H		CH	CH ₃		45 ± 14	117 ± 23
CDD-3164 (4p)	H	H		CH	CH ₃		39 ± 7	96 ± 8
CDD-3165 (4q)	H	H		CH	CH ₃		NA	NA
CDD-3166 (4r)	H	H		CH	H		2.1 ± 0.6	7.3 ± 0.6
CDD-3167 (4s)	H	H		N	CH ₃		0.38 ± 0.08	0.13 ± 0.06
CDD-3168 (4t)	H	H		CH	OCH ₃		1.7 ± 0.9	9.2 ± 3.3
CDD-3170 (4u)	H	H		CH	CH ₃		NA	NA

NA, not active at 250 nM in the biochemical assay. K_i determined from Z'-LYTE and Adapta inhibition data.

respectively. This corresponded to a threefold increase in potency toward EPHA4 and a sevenfold increase toward EPHA2 relative to CDD-2693. Interestingly, removing the same fluoro and methyl substituents from the indazole parent compound (CDD-2781) resulted in CDD-2968 with K_i values of 0.7 nM to EPHA2 and 9.7 nM to EPH4 and thus having a more than 10-fold selectivity toward EPHA4 over EPHA2.

We next turned our attention toward the B-ring and R₅ position which was the basis of the two original hits from the DEL selection. Removing the methyl (CDD-3163) or hydroxyl groups (CDD-3164) on the phenyl ring (compared to CDD-2967) reduced potency to EPHA2 and EPHA4 by more than two orders of magnitude, whereas converting the hydroxy to the methoxy group (CDD-3165) completely abrogated activity. Docking results indicate that the hydroxyl group located on ring 5 forms hydrogen bonds with Glu670 in EPHA4 and Glu663 in EPHA2. Substituting this hydroxyl group with a methyl group resulted in loss of these pivotal interactions, leading to a notable decrease in activity. Furthermore, the methyl group positioned para to the hydroxyl group on ring 5 contributes to binding by fitting into a hydrophobic pocket formed by alanine and valine amino acids. We also explored analogs focused around the indazole parent compound CDD-2968 and found that omitting the 5-methyl group from the indazole ring (CDD-3074) significantly attenuated activity to EPHA2 (K_i: 53 nM) and EPHA4 (K_i: 17.7 nM). The presence of

this 5-methyl group aligns with the position of the methyl group in CDD-2967 within the predicted binding mode. This suggests that the absence of hydrophobic interactions in this pocket could negatively affect the binding affinity. Alternatively, switching the indazole heterocycle to the indole (CDD-3075), 7-azaindole (CDD-3076), or the pyridine (CDD-3170) abolished all activity. The additional nitrogen in the indazole moiety appears to establish a hydrogen bond with Ser763 in EPHA4 and Ser756 in EPHA2, suggesting the importance of this interaction in maintaining the binding pose. Removal of the methyl group at the R₄ (CDD-3166) resulted in a more than 10-fold loss in potency to EPHA2 and EPHA4 as did the introduction of an electron-donating methoxy group (CDD-3168). However, conversion of the phenyl ring to the pyridine (CDD-3167) gave excellent activity toward EPHA2 (K_i: 0.13 nM) and EPHA4 (K_i: 0.38 nM). Altogether, based on these SAR studies, CDD-2967 and CDD-3167 emerged as the potent inhibitors of EPHA2/EPHA4.

Metabolic Stability Analysis. During the lead optimization, we evaluated the metabolic stability of selected potent compounds in mouse/human liver microsomes (MLM/HLM) (Table 3). Our DECL-generated hit compound CDD-2693 showed acceptable stability in MLM ($t_{1/2} = 37$ min) and excellent stability in HLM ($t_{1/2} = 121$ min). Additionally, CDD-2781 with the methyl-indazole

(R₅) motif displayed diminished metabolic stability in MLM ($t_{1/2} = 27$ min) but exceptional stability in HLM ($t_{1/2} = 518$ min). Upon removal of the fluoro group (CDD-2905), the stability was reduced in both MLM ($t_{1/2} = 10$ min) and HLM ($t_{1/2} = 114$ min) compared to CDD-2693. Unfortunately, when the methyl and fluoro substituents were removed from the A-ring (CDD-2967 and CDD-2968), the half-lives dropped to less than 10 min in MLM and less than 100 min in HLM. When the N-methylpiperidine-4-carboxamide was replaced with the smaller N-methylcarboxamide (and CDD-2970), the microsomal stability dramatically improved for CDD-2969 (MLM: $t_{1/2} = 42$ min; HLM: $t_{1/2} = 412$ min) and CDD-2970 (MLM: $t_{1/2} = 38$ min; HLM: $t_{1/2} = 467$ min). The most potent pyridine analog, CDD-3167, was unstable in both MLM and HLM (MLM: $t_{1/2} = 9$ min; HLM: $t_{1/2} = 29$ min). In summary, all the active EPHA2/EPHA4 analogs tested had a $t_{1/2}$ in MLM of less than 45 min and were more stable in HLM, with some analogs being remarkably stable ($t_{1/2}$ of greater than 2 h).

NanoBRET™ Target Engagement Intracellular Kinase Analysis. To determine the cellular potency and selectivity, we evaluated a series of potent compounds in cell-based NanoBRET Intracellular Kinase assays (Promega). This assay determines the apparent affinity of test compounds by competitively dislodging the NanoBRET tracer that is reversibly attached to a NanoLuc luciferase kinase fusion in living cells. We evaluated our compounds against EPH receptors EPHA2, EPHA4, EPHA5, and EPHB2 and off-target kinases SRC, FGR, and YES1 (Table 4). Dasatinib was used as

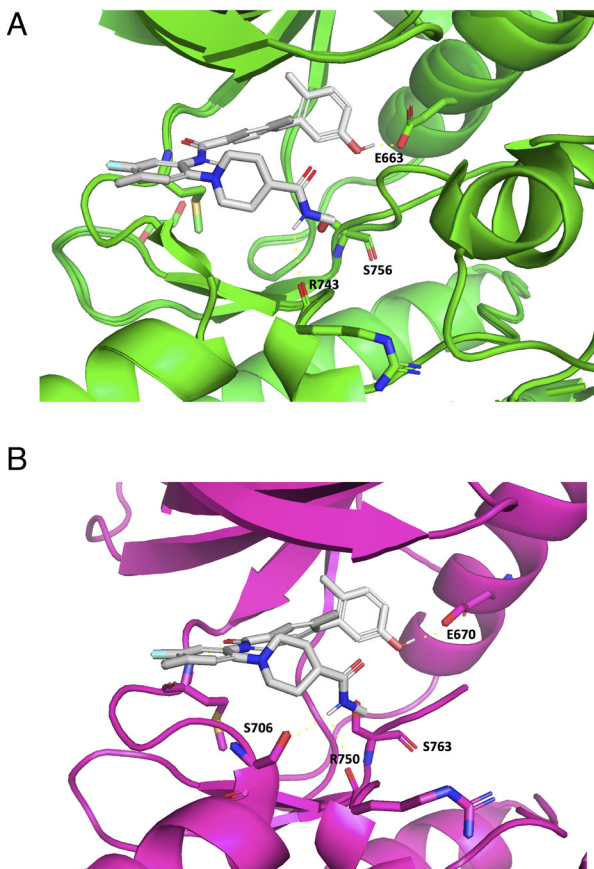


Fig. 5. (A) Computational modeling of EPHA2/CDD-2693 interaction. CDD-2693 forms critical interactions with residues E663, M695, and R743. EPHA2 was shown in green cartoon; CDD-2693 was shown in gray stick. Residues involved in interaction were shown in green stick. (B) Computational modeling of EPHA4/CDD-2693 interaction. CDD-2693 forms critical interactions with residues E670, M702, S706, and R750. EPHA4 was shown in magenta cartoon; CDD-2693 was shown in gray stick. Residues involved in interaction were shown in magenta stick.

a positive control in this assay. The results of the NanoBRET experiments demonstrated that remarkably, seven of the inhibitors (CDD-2693, CDD-2781, CDD-2967, CDD-2968, CDD-2905, and CDD-3167) exhibited IC₅₀ values below 500 nM (1.0 nM to 460 nM) toward these EPH family members, indicating their ability to enter cells and engage the EPH targets. The cellular potency of our qDOS28_1 hit compound CDD-2693 was below 100 nM cellular efficacy against EPHA4 (IC₅₀: 39.6 nM), EPHA5 (IC₅₀: 52.7 nM), and EPHB2 (IC₅₀: 69.9 nM) but showed 460 nM potency against EPHA2 (i.e., 11-fold selective versus EPHA4). A similar selectivity pattern was observed for qDOS26 hit compound CDD-2781 EPHA4 (IC₅₀: 40 nM), EPHA5 (IC₅₀: 38.0 nM), EPHB2 (IC₅₀: 60.0 nM), and EPHA2 (IC₅₀: 159.0 nM) (i.e., fourfold selective). CDD-3167, our most potent analog in vitro, showed single-digit nanomolar potency in cells against EPHA2 (IC₅₀: 8.0 nM), EPHA4 (IC₅₀: 2.3 nM), EPHA5 (IC₅₀: 3.0 nM), and EPHB2 (IC₅₀: 5.2 nM). The cellular potency of CDD-2693 (and all analogs tested) against off-target kinases SRC, YES1, and FGR was in the micromolar range (Table 4), unlike dasatinib, which showed IC₅₀ values of 19 nM, 16 nM, and 41 nM, respectively, against these three kinases. The NanoBRET target engagement results concluded that our developed inhibitors had tremendous cellular selectivity compared to dasatinib.

CDD-2693 and CDD-3167 Inhibited Ephrin-Mediated Activation of Ephrin Receptors in Mammalian Cells and Endometrial Organoids. Building upon our in vitro assays, we also characterized the cellular effects of our newly identified ephrin receptor inhibitors. We used an immortalized human endometriotic cell line (48), 12Z and an Ewing's sarcoma cell line, A673, to examine the phosphorylation of EPHAs upon our inhibitor treatment. To further mimic the biological activation of the EPHAs, cells were treated with EFNA5, a potent ligand for both EPHA2 and EPHA4 (4), in the presence or absence of the inhibitors. We chose hit compound CDD-2693 and potent analog CDD-3167 for further experiments based on their potency in cell-based assays. 12Z cells were pretreated with inhibitors for 15 min followed by the addition of 0.5 μg/mL of EFNA5 for a total of 30 min. Both CDD-2693 and CDD-3167 inhibited the EFNA5-induced phosphorylation of EPHA2/4 (Y772/Y779) in a dosage-dependent manner (Fig. 6A). Further statistical analysis of the signal intensities revealed that CDD-2693 significantly inhibited the phosphorylation starting at 1 μM concentration, while a decreasing trend could be observed at 100 nM with a *P* value of 0.06. CDD-3167 is more potent, showing a significant inhibition effect starting at 1 nM concentration (Fig. 6B). Such an inhibition effect was also observed in the A673 cells, starting at 1 μM (CDD-2693) and 100 nM (CDD-3167) (Fig. 7 A and B). Additionally, we tested the 12Z and A673 cell viability upon the inhibitor treatment. In 12Z cells, CDD-2693 and CDD-3167 both suppressed cell growth at a half-maximal inhibitory concentration (IC₅₀) of 2,831 and 456.3 nM, respectively (Fig. 6C). In A673 cells, IC₅₀ for CDD-2693 is 8,755 nM, and CDD-3167 has an IC₅₀ of 5,085 nM (Fig. 7C).

One of the hallmarks of endometriosis is inducing a proinflammatory state in the microenvironment of the ectopic lesions (49–51) and previous studies in the ovary have shown that ephrin signaling controls expression of the proinflammatory gene, *PTGS2* (18). To test the therapeutic potential of our inhibitors in the context of inflammation, we treated 12Z cells with IL-1β in the presence or absence of CDD-2693 and CDD-3167. After pretreatment of the CDD-2693 and CDD-3167 compounds for 30 min, IL-1β was added to the culturing medium to a final concentration of 0.05 ng/mL. RNA was collected after a 3-h incubation and subjected to reverse transcription quantitative real-time PCR (RT-qPCR) to

Table 3. Metabolic stability of selected compounds in MLM and HLM

Series	Compounds	Assay (half-life)*		MLM CL _{int} (μ L/min/mg)	HLM CL _{int} (μ L/min/mg)
		MLM t _{1/2} (min)	HLM t _{1/2} (min)		
qDOS28_1 and qDOS26	CDD-2693	37	121	37	11
	CDD-2781	27	518	50	2.7
	CDD-2905	10	114	142	12
	CDD-2967	6	37	230	37
	CDD-2968	6	76	245	18
	CDD-2969	42	412	33	3
	CDD-2970	38	467	36	3
	CDD-3167	9	29	156	48
	Alprazolam	296	832	5	2
Control	JQ1	12	9	117	143

*t_{1/2} measured using the liver microsomal stability assay; MLM/HLM, mouse/human liver microsomes; CL, intrinsic clearance.

evaluate the transcript level of *PTGS2*, a known downstream target of IL-1 β to initiate immunoinflammatory responses (52). As shown in Fig. 6*D*, both CDD-2693 and CDD-3167 decreased the *PTGS2* expression in the presence of IL-1 β , with an IC₅₀ of 7.2 μ M and 1.3 μ M, respectively.

Patient-derived organoids grown in three-dimensional cultures have become useful platforms to test the biological effects of drug-like molecules (53), especially in the field of endometrial biology (54, 55). We established endometrial epithelial organoids obtained from hysterectomies of individuals with endometriosis following previously published conditions (54, 56). Four days after plating, epithelial organoids were treated with 5 μ M of CDD-2693 and CDD-3167 and allowed to grow over the course of 72 h (Fig. 6*E* and *F*). Unlike the vehicle-treated organoids, which continued to expand in diameter over the course of the experiment, organoids treated with the ephrin receptor inhibitors, CDD-2693 and CDD-3167, showed a significant decrease in diameter after 72 h of treatment. These results show that CDD-2693 and CDD-3167 significantly decrease the average diameter and the expansion of patient-derived organoids over a 3-d treatment in a patient-derived model of endometriosis.

Discussion

Ephrins signal through their corresponding EPH receptors to control cellular communication and influence cellular processes. Using our DEC-Tec platform, we identified a series of pan-ephrin receptor kinase inhibitors. Initially, we employed efficient on-DNA compatible chemistries to synthesize diverse structural chemical libraries, and after the affinity selection directly yielded two high count DECL selection hit compounds CDD-2693 and CDD-2781 from qDOS28_1 and qDOS26 libraries, respectively. These hits were synthesized off-DNA and their kinase potency against EPHA4 and EPHA2 isoforms was determined. These two compounds (CDD-2693 and CDD-2781) displayed effective biochemical potency on tested kinases with below 10 nM level of inhibition, especially CDD-2693, which showed picomolar efficacy with a K_i value of 0.8 nM against EPHA4. Due to the excellent potency of these hits, we further studied the kinase selectivity more broadly. We determined the selectivity profile using a 468 human kinase panel and demonstrated that CDD-2693 showed excellent inhibition against the EPH family, especially outstanding potency on EPHA4, EPHA2, EPHA5, EPHB2, but no isoform selectivity, CDD-2693 also showed binding activities to SRC, FGR, and YES1 kinases. From these experiments, we conclude that DEC-Tec is an especially useful platform for generating potent and selective inhibitors of biologically validated kinase targets.

To further optimize the hit compound CDD-2693, we synthesized several analogs to acquire SAR. During these studies, we found more potent inhibitors, including CDD-2905, CDD-3167, and CDD-2967, demonstrating potency below 5 nM. To determine the molecular effects of these compounds, we assessed the cellular potency of the most powerful selective compounds using the NanoBRET intracellular kinase assay against EPH and SRC family members. Remarkably, CDD-3167 and CDD-2693 selectively displayed significant cellular potency against EPHA2, EPHA4, EPHA5, and EPHB2, but did not show appreciable cellular activity on SRC, FGR, and YES1 off-targets. Taken together, we conclude that these potent inhibitors demonstrate exceptional selectivity toward EPH family members versus SRC family members. Additionally, we tested the metabolic stability of hit compounds, including their selected analogs, utilizing a human/mouse liver microsomal assay. The half-life of CDD-2693, CDD-2781, CDD-2969, and CDD-2970

Table 4. NanoBRET target engagement data against EPH and SRC, YES1, and FGR kinases

Compounds	NanoBRET data (IC ₅₀ in nM)						
	EPHA2	EPHA4	EPHA5	EPHB2	SRC	YES1	FGR
Dasatinib	6.9	3.4	5.5	6.6	19	16	41
CDD-2693	460.7	39.6	52.7	69.9	21,016	8,661	6,510
CDD-2781	159	40	38	60	10,554	8,828	4,577
CDD-2905	39	10	15	27	8,089	9,404	4,393
CDD-2967	33.2	5.6	10.8	15.4	ND	12,881	5,443
CDD-2968	29	13	13	28	6,244	10,918	5,671
CDD-2969	1,133	227	335	648	5,307	ND	45,616
CDD-2970	434	173	160	294	5,922	27,539	34,529
CDD-3074	10,196	1,859	1,881	4,347	–	–	–
CDD-3163	133,101	11,872	15,647	132,836	–	–	–
CDD-3164	11,915	3,859	3,766	13,470	–	–	–
CDD-3166	663.6	64.8	54.5	206.7	ND	ND	ND
CDD-3167	8	2.3	3	5.2	3,338	6,353	545
CDD-3168	109.1	119.2	137.9	276.3	ND	ND	ND

–, not tested; ND, not determined (IC₅₀ > 50,000 nM).

had a significant improvement in metabolic stability over 120 min on HLMs and a notable stability over 25 min on MLMs.

These inhibitors have the potential to target a major vulnerability in numerous pathologies – from benign conditions such as endometriosis to malignant cancers. We highlight the fact that EPHs are overexpressed and may serve as powerful therapeutic targets. Our study first reported the overexpression of EPHs in endometriosis and correlated the expression levels with the disease invasiveness. We also emphasized the specific niche for the advancement of nonhormonal therapeutic agents for managing pain syndrome and infertility issues in patients suffering from endometriosis. Additionally, in gynecological cancers, EPHs and their ligands are up-regulated in both endometrial and ovarian cancers (15, 57–62). Higher EPHA2 expression level is correlated with more advanced disease stages and poorer survival rates in endometrial cancer patients (15, 62). In ovarian cancer patients, EPHA1/2/4/8 have all been reported to be up-regulated and linked with adverse clinical prognosis (57–59, 63, 64). Prior literature on Ewing sarcoma also identifies EPHA2 as an oncogenic driver of therapeutic significance (23, 24). In addition to cancers, EPHs are also indispensable in multiple physiological processes of reproduction, such as implantation (14, 65) and placentation (66, 67). Thus, perturbed ephrin-EPHs signaling pathways are observed in severe pregnancy complications, namely tubal pregnancies (68, 69) and preeclampsia (70–72). Inhibitors targeting EPHs can also be valuable tools in advancing the mechanistic studies of ephrin-EPHs signaling pathways during developmental events.

Given the profound detrimental effects of EPHs in both physiological and disease conditions, and the limited interventions or perturbation tools available, there is a dire need for the development of innovative compounds and therapies targeting EPHs. In this study, we refined the categories of EPH inhibitors in a high-throughput manner and bridged the gap of potent pan-ephrin receptor kinase inhibitors by developing two pan-EPH inhibitors and exemplified their efficacy in the biological context of endometriosis and Ewing sarcoma.

Materials and Methods

Methods and procedures for the synthesis of compounds, DEC-Tec affinity selection, biochemical assays, NanoBRET™ kinase target engagement intracellular assay, thermal shift assay, and metabolic stability assay are available in *SI Appendix*.

Analysis of EPHA2 and EPHA4 from Patient Tissues. We assessed gene expression in GSE141549 to evaluate expression of genes encoding kinases that were up-regulated in human endometriotic lesion specimens compared to normal and patient eutopic endometrium. The dataset represents specimens from CE (N = 43); PE, (N = 104); PeL, (N = 71); DiE (N = 167); and OMA (N = 25). Datasets are presented as box and whisker plots of the log2Expression (mean, with min-max expression). Lesion expression of *EPHA2* and *EPHA4* was evaluated using multiple testing with an *FDR* < 0.05 of each condition (PeL, OMA, DiE) versus CE. Analysis of *EPHA2* and *EPHA4* in endometrial biopsies from the normal eutopic endometrium was performed in a previously published dataset (GSE51981). The tissues represent specimens obtained from proliferative endometrium (PE, N = 20); early secretory endometrium (ES, N = 6), and midsecretory endometrium (MS, N = 8). Log2 expression data for *EPHA2* and *EPHA4* were plotted as mean, with min-max expression, and were analyzed by a one-way ANOVA with a Tukey's postcomparison test.

Analysis of EPHA2 and EPHA4 Variants in the FinnGen Database. *EPHA2* and *EPHA4* genetic variants associated with endometriosis were identified by mining the FinnGen database (46). Datasets associated with the following phenotypes were obtained: N14_ENDOMETRIOSIS (N = 10,029, control cases, N = 81,593); N14_ENDOMETRIOSIS_OVARY (N = 3,889, control cases, N = 81,593); N14_ENDOMETRIOSIS_PELVICPERITONEUM (N = 3,620, control cases, N = 81,593); N14_ENDOMETRIOSIS_RECTPVAGSEPT_VAGINA (N = 1,626, control cases, N = 81,593); N14_ENDOMETRIOSIS_UTERUS (N = 2,866, control cases, N = 81,593); and N14_ENDOMET_INFERT (N = 1,956, control cases, N = 83,912). *EPHA2* and *EPHA4* variants associated with endometriosis were calculated using *P* < 0.001 and *P* < 0.01.

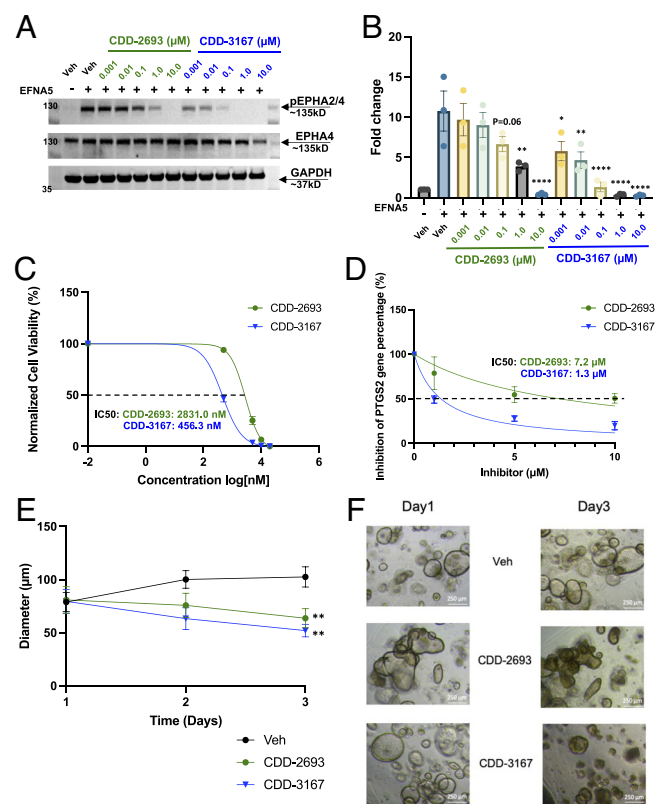


Fig. 6. Inhibited activation of EPHAs upon lead compound treatment in 12Z cells. (A) Western blot showing the inhibition of EPHA2/4 phosphorylation after treatment with 0.5 μ g/mL Ephrin-A5 (EFNA5) for 15 min in the presence or absence CDD-2693 and CDD-3167. (B) Densitometric analysis of (A), fold changes were calculated toward vehicle treatment without EFNA5 stimulation, GAPDH intensities were used as normalizing internal control. ($N = 3$ biological replicates, one-way ANOVA with Tukey's post hoc analysis, plotted as means \pm SEM. **** P < 0.0001. *** P < 0.001. * P < 0.05). (C) Cell viability assay in 12Z cells upon CDD-2693 and CDD-3167 treatment after 72 h incubation. IC_{50} was calculated by nonlinear fit analysis model using GraphPad Prism. (D) PTGS2 gene expression assay in 12Z cells after 3 h IL-1B challenging. Data were normalized toward vehicle treatment with IL-1B stimulation. IC_{50} was calculated by the nonlinear fit analysis model using GraphPad Prism. (E) Endometrial organoid growth curve measured by diameter over a 3-d treatment of CDD-2693. (F) Bright-field images of endometrial organoids after 5 μ M inhibitor treatment from day 1 (Left) to day 3 (Right).

cases, $N = 81,593$; N14_ENDOMETRIOSIS_OVARY ($N = 3,889$, control cases, $N = 81,593$); N14_ENDOMETRIOSIS_PELVICPERITONEUM ($N = 3,620$, control cases, $N = 81,593$); N14_ENDOMETRIOSIS_RECTPVAGSEPT_VAGINA ($N = 1,626$, control cases, $N = 81,593$); N14_ENDOMETRIOSIS_UTERUS ($N = 2,866$, control cases, $N = 81,593$); and N14_ENDOMET_INFERT ($N = 1,956$, control cases, $N = 83,912$). *EPHA2* and *EPHA4* variants associated with endometriosis were calculated using *P* < 0.001 and *P* < 0.01.

Computational Modeling of Binding Poses of CDD-2693 Derivatives in the ATP-binding Pockets of EPHA2 and EPHA4. EPHA2 (PDB ID: 5I9Y) and EPHA4 (PDB ID: 2Y6O) crystal structures were retrieved from the protein data bank (PDB). The proteins were prepared using Schrodinger Suite Release 2022-1 (73) with default settings. A grid for each protein was generated at the site of the ligand in the crystal structure. CDD-2693 and its derivative compounds were prepared using the LigPrep program (74). 3D conformations and protonation states were generated with the Epik program (75). The processed compounds were then docked into the ATP-binding pockets of the two proteins using Glide in the extra precision mode (76). The acquired poses were visualized and analyzed using Maestro and PyMOL program (77).

Immunohistochemistry of EPHA2 in the Normal Endometrium and Endometriotic Lesions. The normal endometrium (proliferative phase, ProEN, $N = 5$; early secretory, ESE, $N = 4$; midsecretory, MSE, $N = 5$) and endometriotic lesions (peritoneal, PeL, $N = 3$; deep infiltrating, DiE, $N = 6$; endometrioma, OMA, $N = 10$) were provided by a board-certified gynecological pathologist who also

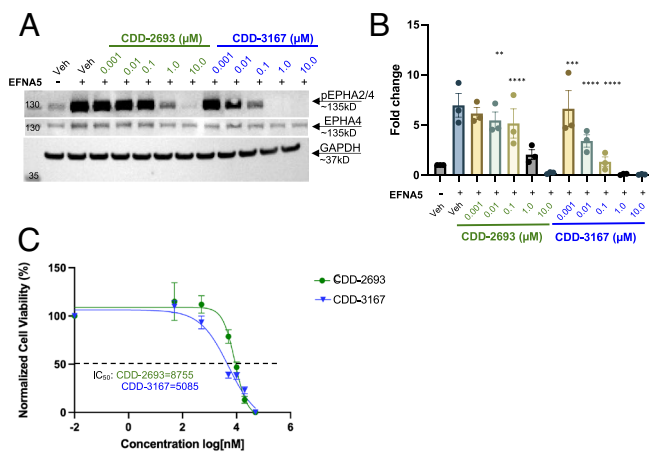


Fig. 7. Inhibited activation of EPHAs upon active compound treatment in A673 cells. (A) Western blot showing the inhibition of EPHA2/4 phosphorylation after treatment with 0.5 μ g/mL Ephrin-A5 (EFNA5) for 15 min in the presence or absence CDD-2693 and CDD-3167. (B) Densitometric analysis of (A); fold changes were calculated based on vehicle treatment without EFNA5 stimulation, and GAPDH intensities were used as a normalizing internal control. ($N = 3$ biological replicates, one-way ANOVA with Tukey's post hoc analysis, plotted as means \pm SEM. **** $P < 0.0001$. *** $P < 0.001$. * $P < 0.05$). (C) Cell viability assay in A673 cells upon CDD-2693 and CDD-3167 treatment after 72 h incubation (CDD-2693: $N = 3$ biological replicates, CDD-3167: $N = 4$ biological replicates). IC₅₀ was calculated by nonlinear fit analysis model using GraphPad Prism.

reviewed EPHA2 staining results. Fixed paraffin-embedded tissues underwent antigen retrieval in 10 mM citrate buffer with 0.5% Tween, pH 6.0, in a microwave for 20 min. After cooling on ice for 30 min while submerged in antigen retrieval buffer, endogenous peroxides were neutralized with a 10 min incubation in hydrogen peroxide, blocked with avidin and biotin, and blocked in 3% BSA for 60 min at room temperature. Sections were incubated with primary antibody (EPHA2, R&D Cat. # AF3035, 1:20 dilution) diluted in 3% BSA and incubated overnight at 4 °C. The following morning, the primary antibody was detected with a biotinylated secondary antibody followed by incubation with a signal amplification avidin/biotin complex (Vector Labs, PK-6100) and developed with DAB peroxidase substrate (Vector Labs, SK-4100). Sections were counterstained with hematoxylin (Sigma), dehydrated, and mounted using Permount mounting medium (VWR). Peroxidase-labeled and H&E-stained slides were imaged using the Aperio AT2 slide scanner (Thomas Huyhn) in the Department of Veterinary Medicine and Surgery at the University of Texas MD Anderson Cancer Center. EPHA2 signal was quantified using ImageJ following a previously published protocol (78) and analyzed using a Kruskal-Wallis test for nonparametric datapoints with a Dunn's multiple comparison posttest to assess the difference between the disease subtypes and endometrial phases.

Evaluation of Small-Molecule Activity in Mammalian Cell Cultures. 12Z cells were acquired from ATCC and maintained in DMEM supplemented with 10% FBS. A673 cells were acquired as a kind gift from Jason Yustein and Atreyi Dasgupta (Baylor College of Medicine, TX) and maintained in DMEM supplemented with 2 mM glutamine and 10% FBS. For small molecules tested with EPHrin-A5 stimulation, 0.6 × 10⁵ cells were seeded on 12-well plates and allowed to attach overnight and change the medium to DMEM supplemented with 2% charcoal-stripped FBS 24 h after seeding. Eighteen hours after medium change, cells were pretreated for 15 min with small-molecule inhibitors at 2× concentration and then supplemented with Ephrin-A5 (R&D Systems, #374-EA-200) to a final concentration of 0.5 μ g/mL for 15 min. Cells were harvested on ice, lysed with 1× LDS sample buffer (Invitrogen, #NP0007), and denatured at 95 °C for 15 min. Then, lysates were electrophoresed by SDS-PAGE gel and probed with pEPHA2/3/4/5 (Cell Signaling, #D10H1), EPHA4 (Invitrogen, #37-1600), and GAPDH (Proteintech, HRP-60004) antibodies. Densitometry analysis was performed using ImageJ (79) and analyzed using GraphPad Prism.

For cell viability assays, cells were plated in the 96-well at the density of 4,000 cells per well to incubate overnight and change the medium to DMEM supplemented with 2% charcoal-stripped FBS 24 h after seeding. Eighteen hours after medium change, cells were treated with corresponding small molecules. Seventy-two hours after the

small-molecule treatment, cell viability was assessed by the CellTiter-Glo Luminescent Assay following the manufacturer's protocol (Promega, #G7570).

For the gene expression assay, 1 × 10⁵ 12Z cells were seeded on 12-well plates and allowed to attach overnight. The medium was changed to DMEM supplemented with 2% charcoal-stripped FBS 24 h after seeding. Eighteen hours after medium change, cells were pretreated for 30 min with small-molecule inhibitors at 2× concentration and then supplemented with IL-1 β (R&D systems, #201-LB-005/CF) to the final concentration to 0.05 ng/mL for 3 h. Total RNAs were subsequently harvested by the RNeasy Kit (QIAGEN, #74004) following the manufacturer's protocol. Reverse transcription was performed using 500 ng of total RNA as input using qScript cDNA SuperMix (Quantabio, #95048-025). The PTGS2 gene was amplified using primers: F-5'CGGTAAACCTGGCTAGACAG3', R-5'GCAACCGTAGATGCTCAGGGA3'. GAPDH was used as the internal control for normalization, with primers: F-5'GTC-TCTCTGACTCACAGCG3', R-5'ACCACCTGTTGCTGTAGCCAA3'. The final fold-change for plotting was calculated compared to vehicle treatment with IL-1 β stimulation.

Studies using human specimens were conducted under the H-21138 protocol approved by the Institutional Review Board at Baylor College of Medicine. Human endometrial epithelial organoids from endometrial tissues of patients with confirmed endometriosis were established as previously described (80). Organoids were plated in Matrigel (Corning Catalog #354230) in a 24-well plate and allowed to grow for 5 d in complete medium [Advanced DMEM/F12 supplemented with 1× N2 supplement (Life Technologies, #17502048), 1× B27 supplement (Life Technologies, #12587010), 100 μ g/mL Primocin (Invivogen, #ant-pm-1), 2 mM L-glutamine (Life Technologies, #25030024), 500 nM A83-01 (Tocris, #2939), 10% R-spondin-1 conditioned media (obtained from the Center for Digestive Diseases, Baylor College of Medicine), 10 nM Nicotinamide (Sigma, #N0636-100G), 1.25 mM N-acetyl-L-cysteine (Sigma, #A9165-5G), 10% NOGGIN conditioned media (obtained from the Center for Digestive Diseases, Baylor College of Medicine), 100 ng/mL FGF10 (Peprotech, #100-26), 50 ng/mL HGF (Peprotech, #120-38), 50 ng/mL EGF (Peprotech, #AF100-15), and 10% WNT3a conditioned media (obtained from the Center for Digestive Diseases, Baylor College of Medicine). Fully formed organoids were then treated with 5 μ M of CDD-2693 and CDD-3167 for a total of 72 h. For the small-molecule treatments, organoids were cultured in minimal differentiation medium [Advanced DMEM/F12 supplemented with 1× N2 supplement (Life Technologies, #17502048), 1× B27 supplement (Life Technologies, #12587010), and 100 μ g/mL Primocin (Invivogen, #ant-pm-1)]. Organoid diameters were analyzed by ImageJ (79).

KINOMEscan Analysis. The KINOMEscan™ Profiling Service from Eurofins/DiscoverX provided the TRESpot kinase dendrogram showing the kinase selectivity profile of the hit compound (CDD-2693) against 468 kinases (31, 47).

Data, Materials, and Software Availability. All study data are included in the article and/or *SI Appendix*.

ACKNOWLEDGMENTS. We thank Xuan Qin and Jian Wang for their assistance in generating the metabolic stability and High Resolution Mass Spectrometry data for this study. This research is supported by the Eunice Kennedy Shriver National Institute of Child Health and Human Development [grants R33HD099995 (F.L.), R01HD105800, HD096057 (D.M.), and R01HD110038 (M.M.M.)]. D.M. is supported by a Next Gen Pregnancy Award from the Burroughs Wellcome Fund (NGP10125). C.J.C. is supported by the Dan L. Duncan Comprehensive Cancer Center Division of Biostatistics, Baylor College of Medicine, Houston, TX 77030; Human Genome Sequencing Center, Baylor College of Medicine, Houston, TX 77030; Department of Medicine, Baylor College of Medicine, Houston, TX 77030; and Department of Obstetrics and Gynecology, Baylor College of Medicine, Houston, TX 77030.

Author affiliations: ^aDepartment of Pathology and Immunology, Baylor College of Medicine, Houston, TX 77030; ^bCenter for Drug Discovery, Baylor College of Medicine, Houston, TX 77030; ^cDepartment of Molecular and Human Genetics, Baylor College of Medicine, Houston, TX 77030; ^dDepartment of Biochemistry and Molecular Pharmacology, Baylor College of Medicine, Houston, TX 77030; ^eDan L. Duncan Comprehensive Cancer Center Division of Biostatistics, Baylor College of Medicine, Houston, TX 77030; ^fHuman Genome Sequencing Center, Baylor College of Medicine, Houston, TX 77030; ^gDepartment of Medicine, Baylor College of Medicine, Houston, TX 77030; and ^hDepartment of Obstetrics and Gynecology, Baylor College of Medicine, Houston, TX 77030

Author contributions: C.M., Z.L., S.E.P., K.L.S., K.M.B., Q.Y., F.L., M.P., Z.T., F.Y., C.J.C., S.T., R.P.M., D.W.Y., D.M., and M.M.M. designed research; C.M., Z.L., S.E.P., K.L.S., K.M.B., F.L., M.P., Z.T., F.Y., C.J.C., S.T., and D.M. performed research; C.M. and X.G. contributed new reagents/analytic tools; C.M., Z.L., S.E.P., K.L.S., K.M.B., Q.Y., F.L., M.P., Z.T., F.Y., C.J.C., S.T., R.P.M., D.W.Y., and D.M. analyzed data; and C.M., Z.L., S.E.P., K.L.S., K.M.B., Q.Y., F.L., M.P., Z.T., F.Y., S.T., D.W.Y., D.M., and M.M.M. wrote the paper.

- A. Poliakov, M. Cotrina, D. G. Wilkinson, Diverse roles of eph receptors and ephrins in the regulation of cell migration and tissue assembly. *Dev. Cell* **7**, 465–480 (2004).
- T. K. Niethammer, J. O. Bush, Getting direction(s): The Eph/ephrin signaling system in cell positioning. *Dev. Biol.* **447**, 42–57 (2019).
- K. K. Murai, E. B. Pasquale, Eph/ephrin signaling: Forward, reverse and crosstalk. *J. Cell Sci.* **116**, 2823–2832 (2003).
- T. K. Darling, T. J. Lamb, Emerging roles for Eph receptors and ephrin ligands in immunity. *Front. Immunol.* **10**, 1473 (2019).
- J. Egea, R. Klein, Bidirectional Eph-ephrin signaling during axon guidance. *Trends Cell Biol.* **17**, 230–238 (2007).
- K. O. Lai, N. Y. Ip, Synapse development and plasticity: Roles of ephrin/Eph receptor signaling. *Curr. Opin. Neurobiol.* **19**, 275–283 (2009).
- K. Ellis, D. Munro, J. Clarke, Endometriosis is undervalued: A call to action. *Front. Glob. Womens Health* **3**, 902371 (2022).
- L. Saavalainen *et al.*, Risk of gynecologic cancer according to the type of endometriosis. *Obstet. Gynecol.* **131**, 1095–1102 (2018).
- P. Vercellini, P. Vigano, E. Somigliana, L. Fedele, Endometriosis: Pathogenesis and treatment. *Nat. Rev. Endocrinol.* **10**, 261–275 (2014).
- C. To *et al.*, Hypoxia-controlled EphA3 marks a human endometrium-derived multipotent mesenchymal stromal cell that supports vascular growth. *PLoS One* **9**, e112106 (2014).
- H. Fujiwara *et al.*, Promoting roles of embryonic signals in embryo implantation and placentation in cooperation with endocrine and immune systems. *Int. J. Mol. Sci.* **21**, 1885 (2020).
- Y. Fu, J. Fu, Q. Ren, X. Chen, A. Wang, Expression of Eph A molecules during swine embryo implantation. *Mol. Biol. Rep.* **39**, 2179–2185 (2012).
- Y. Fu *et al.*, Investigation of Eph-ephrin A1 in the regulation of embryo implantation in sows. *Reprod. Domest. Anim.* **53**, 1563–1574 (2018).
- H. Fujii *et al.*, Eph-ephrin A system regulates murine blastocyst attachment and spreading. *Dev. Dyn.* **235**, 3250–3258 (2006).
- A. A. Kamat *et al.*, EphA2 overexpression is associated with lack of hormone receptor expression and poor outcome in endometrial cancer. *Cancer* **115**, 2684–2692 (2009).
- L. D. Dong *et al.*, Overexpression of erythropoietin-producing hepatocyte receptor B4 and ephrin-B2 is associated with estrogen receptor expression in endometrial adenocarcinoma. *Oncol. Lett.* **13**, 2109–2114 (2017).
- I. Psilopatis, A. Pergaris, K. Vrettou, G. Tsourouflis, S. Theocharis, The EPH/Ephrin system in gynecological cancers: Focusing on the roots of carcinogenesis for better patient management. *Int. J. Mol. Sci.* **23**, 3249 (2022).
- A. V. Buensuceso *et al.*, Ephrin-A5 is required for optimal fertility and a complete ovulatory response to gonadotropins in the female mouse. *Endocrinology* **157**, 942–955 (2016).
- R. Hudecek, B. Kohlova, I. Siskova, M. Piskacek, A. Knight, Blocking of EphA2 on endometrial tumor cells reduces susceptibility to Vdelta1 gamma-delta T-cell-mediated killing. *Front. Immunol.* **12**, 752646 (2021).
- E. A. Adu-Gyamfi *et al.*, Ephrin and Eph receptor signaling in female reproductive physiology and pathology. *Dagger. Biol. Reprod.* **104**, 71–82 (2021).
- E. B. Pasquale, Eph receptors and ephrins in cancer: Bidirectional signalling and beyond. *Nat. Rev. Cancer* **10**, 165–180 (2010).
- N. J. Balamuth, R. B. Womer, Ewing's sarcoma. *Lancet Oncol.* **11**, 184–192 (2010).
- M. Sainz-Jaspeado *et al.*, EphA2-induced angiogenesis in ewing sarcoma cells works through bFGF production and is dependent on caveolin-1. *PLoS One* **8**, e71449 (2013).
- G. Giordano *et al.*, EphA2 expression in bone sarcomas: Bioinformatic analyses and preclinical characterization in patient-derived models of osteosarcoma, Ewing's sarcoma and chondrosarcoma. *Cells* **10**, 2893 (2021).
- N. Cheng *et al.*, Inhibition of VEGF-dependent multistage carcinogenesis by soluble EphA receptors. *Neoplasia* **5**, 445–456 (2003).
- P. Dobrzenski *et al.*, Antiangiogenic and antitumor efficacy of EphA2 receptor antagonist. *Cancer Res.* **64**, 910–919 (2004).
- N. Cheng *et al.*, Blockade of EphA receptor tyrosine kinase activation inhibits vascular endothelial cell growth factor-induced angiogenesis. *Mol. Cancer Res.* **1**, 2–11 (2002).
- L. W. Noblitt *et al.*, Decreased tumorigenic potential of EphA2-overexpressing breast cancer cells following treatment with adenoviral vectors that express EphrinA1. *Cancer Gene Ther.* **11**, 757–766 (2004).
- N. K. Noren, M. Lu, A. L. Freeman, M. Koolpe, E. B. Pasquale, Interplay between EphB4 on tumor cells and vascular ephrin-B2 regulates tumor growth. *Proc. Natl. Acad. Sci. U.S.A.* **101**, 5583–5588 (2004).
- M. Koolpe, M. Dail, E. B. Pasquale, An ephrin mimetic peptide that selectively targets the EphA2 receptor. *J. Biol. Chem.* **277**, 46974–46979 (2002).
- M. W. Karaman *et al.*, A quantitative analysis of kinase inhibitor selectivity. *Nat. Biotechnol.* **26**, 127–132 (2008).
- L. Qiao *et al.*, Structure-activity relationship study of EphB3 receptor tyrosine kinase inhibitors. *Bioorg. Med. Chem. Lett.* **19**, 6122–6126 (2009).
- Y. Choi *et al.*, Discovery and structural analysis of Eph receptor tyrosine kinase inhibitors. *Bioorg. Med. Chem. Lett.* **19**, 4467–4470 (2009).
- R. M. Franzini, D. Neri, J. Scheuermann, DNA-encoded chemical libraries: Advancing beyond conventional small-molecule libraries. *Acc. Chem. Res.* **47**, 1247–1255 (2014).
- Y. K. Sunkari, V. K. Siripuram, T. L. Nguyen, M. Flajole, High-power screening (HPS) empowered by DNA-encoded libraries. *Trends Pharmacol. Sci.* **43**, 4–15 (2022).
- A. L. Satz *et al.*, DNA-encoded chemical libraries. *Nat. Rev. Methods Primers* **2**, 3 (2022).
- A. Gironda-Martinez, E. J. Donckele, F. Samain, D. Neri, DNA-encoded chemical libraries: A comprehensive review with successful stories and future challenges. *ACS Pharmacol. Transl. Sci.* **4**, 1265–1279 (2021).
- J. C. Faver *et al.*, Quantitative comparison of enrichment from DNA-encoded chemical library selections. *ACS Comb. Sci.* **21**, 75–82 (2019).
- J. Zhang, L. Wang, Q. Ji, F. Liu, DNA-Compatible cyanomethylation of (hetero)aryl halides or triflates under a tandem reaction for DNA-encoded library synthesis. *Org. Lett.* **25**, 6931–6936 (2023).
- Z. Yu *et al.*, Discovery and characterization of bromodomain 2-specific inhibitors of BRDT. *Proc. Natl. Acad. Sci. U.S.A.* **118**, e2021102118 (2021).
- R. K. Modukuri *et al.*, Discovery of potent BET bromodomain 1 stereoselective inhibitors using DNA-encoded chemical library selections. *Proc. Natl. Acad. Sci. U.S.A.* **119**, e2122506119 (2022).
- R. K. Modukuri *et al.*, Discovery of highly potent and BMPR2-selective kinase inhibitors using DNA-encoded chemical library screening. *J. Med. Chem.* **66**, 2143–2160 (2023).
- R. Jimmudi *et al.*, DNA-encoded chemical libraries yield non-covalent and non-peptidic SARS-CoV-2 main protease inhibitors. *Commun. Chem.* **6**, 164 (2023).
- M. Gabriel *et al.*, A relational database to identify differentially expressed genes in the endometrium and endometriosis lesions. *Sci. Data* **7**, 284 (2020).
- J. S. Tamaresis *et al.*, Molecular classification of endometriosis and disease stage using high-dimensional genomic data. *Endocrinology* **155**, 4986–4999 (2014).
- M. I. Kurki *et al.*, FinnGen provides genetic insights from a well-phenotyped isolated population. *Nature* **613**, 508–518 (2023).
- M. A. Fabian *et al.*, A small molecule-kinase interaction map for clinical kinase inhibitors. *Nat. Biotechnol.* **23**, 329–336 (2005).
- A. Zeitvogel, R. Baumann, A. Starzinski-Powitz, Identification of an invasive, N-cadherin-expressing epithelial cell type in endometriosis using a new cell culture model. *Am. J. Pathol.* **159**, 1839–1852 (2001).
- J. Arnold *et al.*, Imbalance between sympathetic and sensory innervation in peritoneal endometriosis. *Brain Behav. Immun.* **26**, 132–141 (2012).
- V. Anaf *et al.*, Relationship between endometriotic foci and nerves in rectovaginal endometriotic nodules. *Hum. Reprod.* **15**, 1744–1750 (2000).
- B. D. McKinnon, D. Bertschi, N. A. Bersinger, M. D. Mueller, Inflammation and nerve fiber interaction in endometriotic pain. *Trends Endocrinol. Metab.* **26**, 1–10 (2015).
- E. Molina-Holgado, S. Ortiz, F. Molina-Holgado, C. Guaza, Induction of COX-2 and PGE(2) biosynthesis by IL-1 β is mediated by PKC and mitogen-activated protein kinases in murine astrocytes. *Br. J. Pharmacol.* **131**, 152–159 (2000).
- T. Takahashi, Organoids for drug discovery and personalized medicine. *Annu. Rev. Pharmacol. Toxicol.* **59**, 447–462 (2019).
- M. Y. Turco *et al.*, Long-term, hormone-responsive organoid cultures of human endometrium in a chemically defined medium. *Nat. Cell Biol.* **19**, 568–577 (2017).
- Y. Hibouei, A. Feki, Organoid models of human endometrial development and disease. *Front Cell Dev. Biol.* **8**, 84 (2020).
- M. Boretto *et al.*, Development of organoids from mouse and human endometrium showing endometrial epithelium physiology and long-term expandability. *Development* **144**, 1775–1786 (2017).
- N. I. Herath *et al.*, Over-expression of Eph and ephrin genes in advanced ovarian cancer: Ephrin gene expression correlates with shortened survival. *BMC Cancer* **6**, 144 (2006).
- L. Han *et al.*, The clinical significance of EphA2 and Ephrin A-1 in epithelial ovarian carcinomas. *Gynecol. Oncol.* **99**, 278–286 (2005).
- X. Liu *et al.*, EphA8 is a prognostic marker for epithelial ovarian cancer. *Oncotarget* **7**, 20801–20809 (2016).
- G. Berclaz *et al.*, Activation of the receptor protein tyrosine kinase EphB4 in endometrial hyperplasia and endometrial carcinoma. *Ann. Oncol.* **14**, 220–226 (2003).
- S. M. Alam, J. Fujimoto, I. Jahan, E. Sato, T. Tamaya, Overexpression of ephrinB2 and EphB4 in tumor advancement of uterine endometrial cancers. *Ann. Oncol.* **18**, 485–490 (2007).
- W. M. Merritt *et al.*, Clinical and biological impact of EphA2 overexpression and angiogenesis in endometrial cancer. *Cancer Biol. Ther.* **10**, 1306–1314 (2010).
- S. Reinarz *et al.*, A transcriptome-based global map of signaling pathways in the ovarian cancer microenvironment associated with clinical outcome. *Genome Biol.* **17**, 108 (2016).
- P. H. Thaker *et al.*, EphA2 expression is associated with aggressive features in ovarian carcinoma. *Clin. Cancer Res.* **10**, 5145–5150 (2004).
- H. Fujii, H. Fujiwara, A. Horie, Y. Sato, I. Konishi, Ephrin A1 induces intercellular dissociation in Ishikawa cells: Possible implication of the Eph-ephrin A system in human embryo implantation. *Hum. Reprod.* **26**, 299–306 (2011).
- Y. Yang, J. Min, Effect of ephrin-A1/EphA2 on invasion of trophoblastic cells. *J. Huazhong Univ. Sci. Technol. Med. Sci.* **31**, 824–827 (2011).
- H. Fujiwara *et al.*, Eph-ephrin A system regulates human choriocarcinoma-derived JEG-3 cell invasion. *Int. J. Gynecol. Cancer* **23**, 576–582 (2013).
- X. Y. Yang, W. J. Zhu, H. Jiang, Activation of erythropoietin-producing hepatocellular receptor A2 attenuates cell adhesion of human fallopian tube epithelial cells via focal adhesion kinase dephosphorylation. *Mol. Cell Biochem.* **361**, 259–265 (2012).
- H. Jiang, X. Y. Yang, W. J. Zhu, Dysregulated erythropoietin-producing hepatocellular receptor A2 (EphA2) is involved in tubal pregnancy via regulating cell adhesion of the Fallopian tube epithelial cells. *Reprod. Biol. Endocrinol.* **16**, 84 (2018).
- Y. Zhang *et al.*, Elevated levels of hypoxia-inducible microRNA-210 in pre-eclampsia: New insights into molecular mechanisms for the disease. *J. Cell Mol. Med.* **16**, 249–259 (2012).
- W. Wang *et al.*, Preeclampsia up-regulates angiogenesis-associated microRNA (i.e., miR-17, -20a, and -20b) that target ephrin-B2 and EPHB4 in human placenta. *J. Clin. Endocrinol. Metab.* **97**, E1051–1059 (2012).
- N. Ilan, J. A. Madri, New paradigms of signaling in the vasculature: Ephrins and metalloproteases. *Curr. Opin. Biotechnol.* **10**, 536–540 (1999).
- L. Schrödinger, Schrödinger Release 2022-1 (Schrödinger LLC, New York, NY, 2022).
- L. Schrödinger, Schrödinger Release 2022-1: LigPrep (Schrödinger, LLC, New York, NY, 2022).
- R. C. Johnston *et al.*, Epik: pk(A) and protonation state prediction through machine learning. *J. Chem. Theory Comput.* **19**, 2380–2388 (2023).
- R. A. Friesner *et al.*, Extra precision glide: Docking and scoring incorporating a model of hydrophobic enclosure for protein-ligand complexes. *J. Med. Chem.* **49**, 6177–6196 (2006).
- L. Schrödinger, Schrödinger Release 2023-4: Maestro (Schrödinger, LLC, New York, NY, 2022).
- T. Yang *et al.*, Therapeutic HNF4A mRNA attenuates liver fibrosis in a preclinical model. *J. Hepatol.* **75**, 1420–1433 (2021).
- C. A. Schneider, W. S. Rasband, K. W. Eliceiri, NIH Image to ImageJ: 25 years of image analysis. *Nat. Methods* **9**, 671–675 (2012).
- H. C. Fitzgerald, P. Dhakal, S. K. Behura, D. J. Schust, T. E. Spencer, Self-renewing endometrial epithelial organoids of the human uterus. *Proc. Natl. Acad. Sci. U.S.A.* **116**, 23132–23142 (2019).